Structure-Property Relationships in Single-ion Conducting Multiblock Copolymers: A Phase Diagram and Ionic Conductivities

Jinseok Park^{§, a}, Anne Staiger^{§, b}, Stefan Mecking*, b, Karen Winey*, a

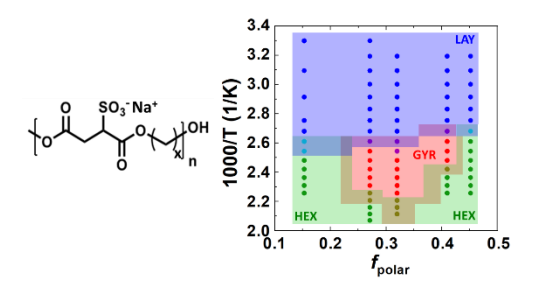
^aDepartment of Materials Science and Engineering, University of Pennsylvania, Philadelphia, Pennsylvania 19104, United States

^bDepartment of Chemistry, University of Konstanz, Universitätsstraße 10, 78457 Konstanz, Germany

E-mail address: winey@seas.upenn.edu

stefan.mecking@uni-konstanz.de

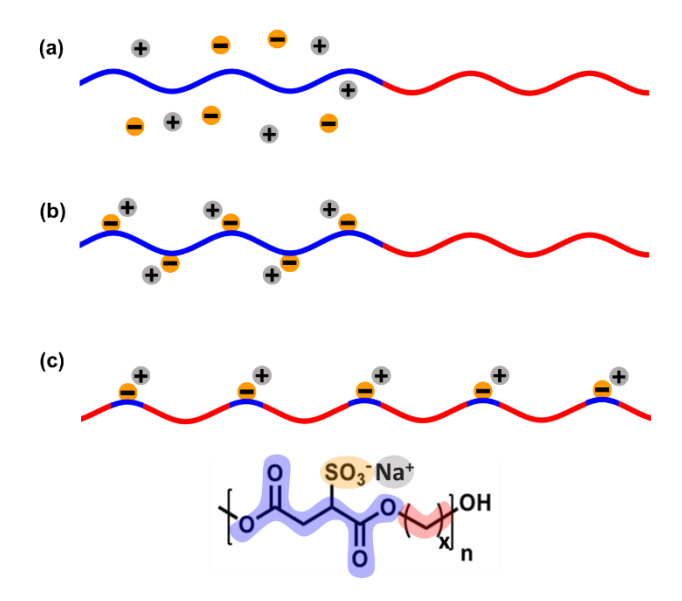
Table of Contents



Abstract

We investigated the nanoscale morphologies and ionic conductivities of polyethylene-based multiblock copolymers as single-ion conducting polymer electrolytes. These polymers contain short polar blocks with a single sodium sulfonate group separated by polyethylene blocks of fixed length (PESxNa, x = 10, 12, 18). At room temperature, these multiblock copolymers exhibit layered ionic aggregates with semicrystalline polyethylene backbones. For PES12Na and PES18Na, the layered ionic aggregate morphologies transition into $Ia\bar{3}d$ gyroid morphologies upon melting the polyethylene blocks, and further transition into hexagonal morphologies at higher temperatures. With a shorter polyethylene block, PES10Na exhibits a layered to hexagonal transition at the melting temperature, without an intermediate gyroid morphology. The phase diagram of these PESxNa polymers is reminiscent of conventional diblock copolymers and identifies the presence of gyroid morphologies at the polar block volume fraction $\sim 0.27 - 0.41$, which is broad compared to typical diblock copolymers. Temperature-dependent ionic conductivities reveal faster ion transport through bicontinuous gyroids than hexagonal ionic aggregate morphologies, and a relationship between conductivity and the characteristic distance between ionic aggregates. This study presents materials design strategies for single-ion conducting polymers with a bicontinuous ionic aggregate and toward efficient ion transport.

Development of solid polymer electrolytes is critical to advanced energy storage technologies (e.g., all-solid-state batteries) beyond the conventional battery systems with liquid electrolytes.^{1–3} The most widely studied solid polymer electrolytes are poly(ethylene oxide) (PEO) based systems with added salt, and include diblock copolymers with a PEO block and a glassy block with Li-salt, Scheme 1a.^{2–6} However, salt-containing polymer electrolytes contain both mobile cations and anions leading to the persistent problems of electrode polarization and low transference numbers.^{2,7} Therefore, single-ion conducting polymer electrolytes (SIPEs) containing immobilized anions on the polymer backbone have emerged as a viable alternative to salt-based polymer electrolytes.^{3,8} Nevertheless, the development of SIPEs remains challenging due to the poor ionic conductivity and limited understanding of structure – property relationships.³



Scheme 1. Schematics of various ion-conducting polymer electrolytes including (a) Li-salt containing diblock copolymers (dual-ion conductors) and (b) anion-tethered diblock copolymers (single-ion conductors). (c) Schematic and molecular structure of PESxNa multiblock copolymers with tethered anion groups. The polar blocks (blue) include one SO_3 -Na⁺ ionic groups. The non-polar blocks (red) are precise polyethylene segments with x = 10 - 48.

The low ionic conductivity of SIPEs is generally attributed to limited cation dissociation from the ion pairs (insufficient free charge carriers) and slow cation mobility due to coupling with segmental relaxations of the polymer backbone. ^{9,10} To improve the cation dissociation, bulky and polar anionic groups are often introduced, because the delocalized electrons of such dielectric anions weakly interact with the cations. ^{7,11} However, interactions between the polar ionic groups slow segmental dynamics of polymer chains and increase the glass transition temperatures (T_g). ^{9,12–14} Therefore, improving the ionic conductivity of SIPEs is often limited due to the anticorrelated relationships between the cation dissociation and segmental relaxation.

Recent studies demonstrate that the characteristics of ionic aggregate morphologies are critical factors in determining ion transport behaviors in SIPEs.^{15–24} For example, a 3D-bicontinuous gyroid morphology exhibits higher Li⁺ conductivities than the hexagonal and layered morphologies due to the interconnected ionic aggregates.¹⁷ Also, well-ordered sulfonic acid layers in a hydrated semicrystalline SIPE shows comparable proton conductivities to Nafion, which was attributed to the highly percolating proton transport domains.²⁵ These studies suggest that there are intricate relationships between the ionic aggregate morphologies, cation dissociation, and polymer chain dynamics, and these factors are largely dictated by the polymer chemistries.^{9,10} Thus, it is critical to design and investigate SIPEs with controlled ionic aggregate morphologies to establish robust morphology – ion transport relationships.

Various polymer chemistries and architectures have been developed to control and investigate the ionic aggregate morphologies of SIPEs. For example, a typical aromatic ionomer with sulfonated ionic groups exhibited poorly defined ionic aggregates due to the constraints imposed by the rigid aromatic backbone.^{26–29} In these highly aromatic polymers, the absence of structural information of ionic aggregate morphologies (e.g., ion-ion correlation length) limits the

investigation of morphology – property relationship.²⁹ Diblock copolymers comprised of aliphatic blocks and SIPE blocks with pendant ionic groups (Scheme 1b), have better defined ionic aggregate morphologies due to enhanced chain flexibility.^{24,30,31} Note that the ionic aggregates in these materials are largely uninvestigated and are smaller than the microphase separated morphologies of the diblock copolymers. The phase behavior of charge-containing diblock copolymers is given by an effective Flory-Huggins interaction parameter (χ_{eff}), the total degree of polymerization of the diblock copolymers, and the relative volumes of the two block, similar to the well-known neutral diblock copolymer systems (e.g., polyisoprene-*b*-polystyrene).^{30,32} The χ_{eff} increases with the ionic composition of the SIPE block, which strengthens the microphase separation as demonstrated in theoretical³⁰ and experimental^{24,31} investigations. Studies of such SIPE block copolymers have identified various ordered morphologies including layered, gyroid, and hexagonal ionic aggregates, although predictive morphology – ion transport relationships require a more detailed understanding of the role of ionic aggregates within the microphase-separated block copolymer morphologies.

We have been studying various SIPEs containing well-separated ionic groups in which the ionic aggregates are synonymous with the microphase separated morphology. When the chain architecture of these polymers has precise segmentation of pendant ionic groups, the ionic aggregates have higher degrees of morphological ordering relative to a random distribution of ionic groups. Specifically, periodic sequencing of carboxylic acid on the polyethylene backbone have greater morphological uniformity of ionic aggregates than the randomly placed carboxylic acid groups.^{33,34} Furthermore, a series of polyethylene-based multiblock copolymer electrolytes containing polar blocks each with one sulfonated ionic group (Scheme 1c) exhibits various order-to-order transitions (OOTs) as a function of temperature.^{17,18} These precisely segmented

polyethylene sulfonates (PESxM) have exactly x carbons in the polyethylene block and M is the counter-ion species. Notably, PES23 with Li⁺, Na⁺, and Cs⁺ counterions have gyroid morphologies with a volume fraction of the polar domain (f_{polar}) ~ 0.28.¹⁷ The temperature range for the gyroid structure shifts with the cation species, which is attributed to the temperature-dependent Coulombic interactions that affect χ_{eff} . A similar multiblock copolymer (PES48Na) with a 48-carbon polyethylene block f_{polar} ~ 0.16 and did not exhibit the gyroid morphology.¹⁸

In this paper, we present a new series of PESxNa multiblock copolymer electrolytes comprised of non-polar polyethylene blocks (x = 10, 12, and 18) and short polar blocks with one SO_3 -Na⁺ ionic group. We establish the phase behavior of PESxNa as a function of f_{polar} and temperature, as well as morphology – conductivity relationships. Notably, the phase diagram of PESxNa multiblock copolymers exhibits the gyroid morphologies at $0.27 < f_{polar} < 0.41$, which is broader than typically reported for diblock copolymers (e.g., polystyrene-b-polyisoprene exhibits the gyroid morphology at $0.37 < f_{PS} < 0.40$). We also highlight the sub-50Å domain spacing of PESxNa polymers and its scaling to the number of backbone atoms in the monomeric repeat unit, and thus demonstrates the ability to control the nanoscale morphologies of ionic aggregates. The controlled ionic aggregate morphologies in PESxNa provide an in-depth structure-property relationship of these SIPEs. Specifically, the higher ionic conductivity in the gyroid morphology relative to the hexagonal morphology correlates with the characteristic length of these morphologies. This study controls the ionic aggregate morphologies and enhanced ionic conductivities using both polymer chemistry and temperature, thereby advancing the fundamental understanding needed to design viable single-ion conducting polymer electrolytes.

EXPERIMENTAL SECTION

Synthesis of materials

PESxNa multiblock copolymer electrolytes were synthesized by step-growth polymerization of tetra-n-butylammonium dimethyl sulfosuccinates (NBu₄DSS) and diols with x-carbons. All reactions were performed under an inert gas atmosphere using standard glovebox and Schlenk techniques. NaCl was supplied by Merck. Dialysis tubes by SpectraPor were provided by Carl Roth and used for purification of the polymers (3.5 kD pore size, 54 mm broadness). 1,18-octadecanediol was synthesized according to literature.³⁵ 1,12-dodecanediol and 1,10-decanediol were purchased from Merck in \geq 98 % purity.

PES10Na and PES12Na: A 100 mL two-necked Schlenk tube was charged with the starting materials of NBu₄SDS (4.62 g, 9.88 mmol, 1.0 eq.) and 1,10-decanediol (1.72 g, 9.88 mmol, 1.0 eq.) or 1,12-dodecanediol (2.00 g, 9.88 mmol, 1.0 eq.) and an elliptical PTFE coated stirring bar with a rare earth magnetic core. The Schlenk tube was equipped with a distillation bridge with one collecting flask and connected to a membrane pump. The reaction mixture was heated to 100 °C until a homogeneous melt was obtained. The catalyst [Ti(OⁿBu)₄] was added as a solution in dry toluene (0.01 M, 0.5 mL, 0.05 mol-%). The reaction mixture was heated to 120 °C and the pressure was slowly reduced to 100 mbar within 5 h. The pressure was then reduced to oil pump vacuo (10⁻² mbar) and the temperature was raised to 160 °C and held for 16 h. To obtain the sodium salt, brine (100 mL) and deionized water (20 mL) were added and the flask was ultrasonicated for 10 minutes until the polymer was dissolved. The solution was dialyzed for three days (5 L deionized water bath, water exchange 3x/day). The solvent was removed by lyophilization and NMR measurement ensured the absence of tetra-n-butylammonium counterions. In the case of remaining tetra-n-butylammonium, the process was repeated. The polymers were

obtained in 80 % yield.

PES18Na: For the synthesis of PES18Na, the published procedure by Rank *et al.* was followed. A 100 mL two-necked Schlenk tube was charged with the starting materials NBu₄DSS (3.50 g, 7.5 mmol, 1.0 eq.) and 1,18-octadecanediol (2.15 g, 7.5 mmol, 1.0 eq.) and a mechanical stirrer with a helical agitator was placed into the tube. The mixture was degassed and flushed with nitrogen three times and heated to 130 °C to obtain a homogeneous melt. The catalyst [Ti(OⁿBu)₄] was added as a 0.01 M solution in toluene (375 μL, 3.75 μmol, 0.05 mol-%) *via* syringe to the stirred solution. The reaction mixture was heated slowly to 160 °C within 4 hours. Vacuum was applied and the reaction mixture was stirred for 20 h. The viscous melt was cooled to room temperature and an NMR sample was taken. To obtain the sodium salt of the polymer, brine (100 mL) and deionized water (20 mL) were added to 1.9 g of the polymer. Upon heating to 60 °C, the polymer started to precipitate in the aqueous solution as a white solid. After the melt was fully dispersed, the precipitate was filtered off and washed with deionized water. It was dried in a vacuum drying oven at 3 mbar for 3 days. The polymer PES18Na was obtained in 84 % yield (1.08 g).

Nuclear Magnetic Resonance (NMR) spectroscopy

The characterization of the soluble intermediate products by NMR spectroscopy was performed in dimethylsulfoxide- d_6 as solvent at 25 °C or 110 °C. A Bruker Avance III HD 400 spectrometer with a TBO probe with Z-gradient or a Bruker Avance III 400 with a BBFO plus probe with Z-gradient was used. ¹H chemical shifts were referenced to the solvent signal (residual proton signal). Multiplicities are reported as follows: s (singlet), d (doublet), t (triplet), m (multiplet), v (virtual), and combinations thereof. MestreNova software by Mestrelab Research S.L. was used for the evaluation of NMR data. All deuterated solvents used for NMR spectroscopy

were supplied by Eurisotop.

Differential Scanning Calorimetry (DSC)

DSC experiments were performed with TA Instruments DSC2500 for all polymers. The powder polymer samples were kept in a vacuum desiccator and dried at 50 °C under vacuum overnight prior to perform DSC measurements. Due to the slow crystallization kinetics, samples were measured at 1 °C/min ramping rate under a nitrogen atmosphere. The measured temperature range varies due to the degradation temperatures, which were ~180 - 210 °C with increasing polyethylene block lengths.

In-situ X-ray Scattering

X-ray scattering experiments were performed in the Dual-source and Environmental X-ray Scattering (DEXS) facility at the Laboratory for Research on the Structure of Matter, University of Pennsylvania. The DEXS facility is equipped with a Xeuss 2.0 from Xenocs, which includes a PILATUS 1M detector for small-angle scattering, a PILATUS 100K detector for wide-angle scattering, and a GeniX3D beam source (8 keV, Cu K α , λ = 1.54 Å). The sample to detector distance of ~370mm and ~158mm is used for the small- and wide-angle detectors, respectively. Powder samples kept in a vacuum desiccator were sealed in a 1.0mm diameter glass capillaries before measurements. The 2D scattering data were collected isothermally every 10 °C for 10 min, after 15 min equilibration. The heating and cooling rates were 10 °C/min. The scattering data was isotropic and integrated into I(q) plots. Small- and wide-angle I(q) plots were arbitrarily shifted to display the scattering data at 0.1 Å⁻¹ < q < 1.8 Å⁻¹.

Electrochemical Impedance Spectroscopy (EIS)

Solartron Analytical Modulab XM MTS spectrometer with Janis VPF-100 cryostat was used to measure the electrochemical impedance of samples at frequencies of 0.1 to 1 MHz and 100 mV amplitude. Hot-pressed polymer films (1cm diameter) were sandwiched between two electrodes and equilibrated at ~170 °C under vacuum in the cryostat. Isothermal frequency-sweep measurements were performed while cooling, every 2 °C with 5 mins equilibration. The bulk resistance (R) at each temperature was obtained from the Nyquist plot, and DC ionic conductivity (σ) was calculated from the polymer thickness (R) and area (R), $\sigma = \frac{h}{A \times R}$.

RESULTS AND DISCUSSION

Materials

Table 1 summarizes the basic properties of the PESxNa polymers. We performed ¹H NMR end-group analysis to estimate the degree of polymerization and molecular weights of the polymers (Figure S1 – S4). To build a phase diagram of PES polymers, volume fractions of polar segments (f_{polar} , Scheme 1c) are calculated from the van der Waals volume using the Chemicalize software. The f_{polar} increases from 0.16 to 0.45 as the number of ethylene units between the sulfosuccinate groups decrease from 48 to 10. We approximate the molecular weight polydispersity to be ~ 2 for the step-growth polymerization, because the polymers are insufficiently soluble to size exclusion chromatography. In contrast to traditional diblock copolymers, the molecular weight dispersity does not impact f_{polar} , because the monomeric repeat units are precise.

Table 1. Basic properties of PESxNa

Polymer	$\mathrm{DP_n}^a$	M_n^a (kg/mol)	$f_{ m polar}{}^b$
PES10Na	71	12.7	0.45
PES12Na	75	14.5	0.41
PES18Na	35	8.2	0.32
PES23Na ^c	21	11.3	0.27
PES48Na ^c	30	13.3	0.16

^aThe degree of polymerization and molecular weight were determined by the end-group analysis of ¹H NMR spectra. ^bThe volume fraction of sulfosuccinate blocks. ^cPES23Na and PES48Na data is obtained from Ref. 17 and Ref. 18, respectively.

Thermal and Morphology Transitions

The PESxNa polymers are semicrystalline at room temperature, exhibiting melting temperatures of 91.7°C, 100.9°C, and 126.2°C for PES10Na, PES12Na, and PES18Na, respectively, Figure 1. The melting temperatures increase with longer polyethylene lengths because longer alkyl spacers have more backbone atoms that can maneuver into crystalline domains in the presence of ionic associations and hairpin turns.²⁵ During the first heating cycle above the melting transition, there are no additional transitions for PES10Na and PES12Na, whereas PES18Na shows a transition peak at 190.5°C. This order-to-order transition (OOT) of PES18Na is reversible as evidenced by the peak at 170.6°C during the first cooling cycle. Upon cooling, the absence of crystallization for these three PESxNa polymers is the result of polar ionic interactions constraining backbone mobility and dramatically slowing recrystallization. As a result, there are no melting transitions during the second heating cycles in these polymers, although the OOT is evident in PES18Na. DSC traces also reveal increasing glass transition temperatures (Tg) with larger f_{polar}, as expected.

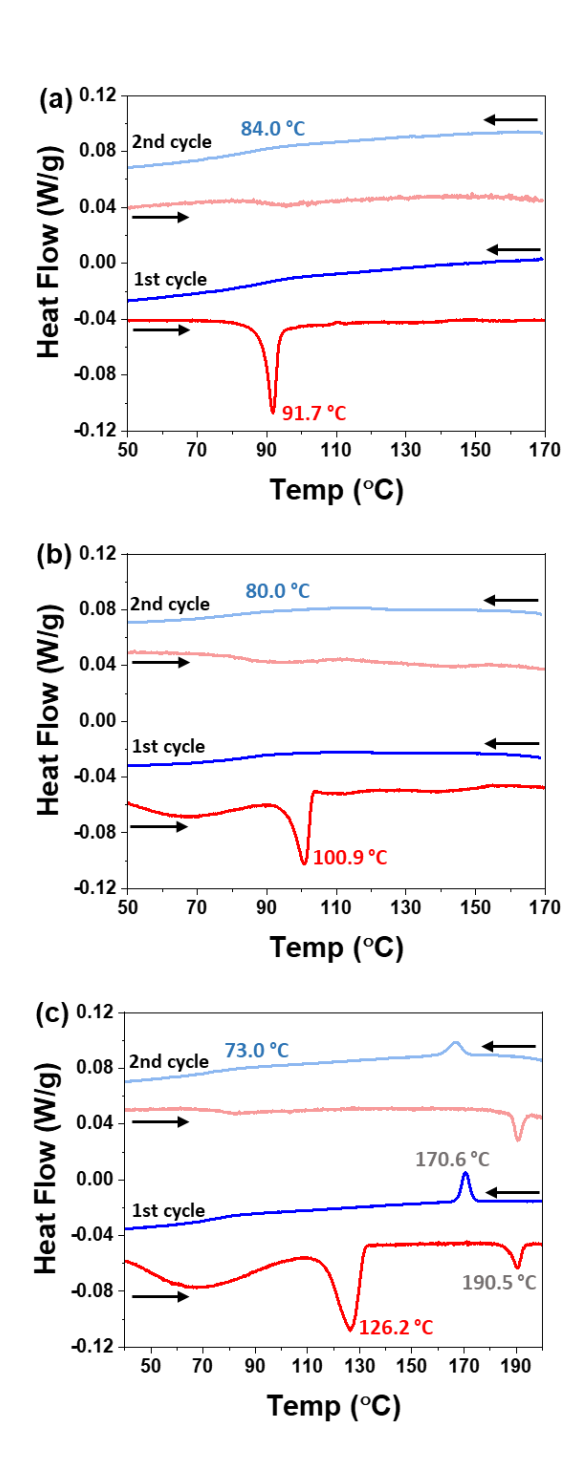


Figure 1. DSC traces of (a) PES10Na, (b) PES12Na, and (c) PES18Na measured at 1°C/min ramp rate, including heating (red) and cooling (blue) of first and second cycles. DSC traces of first and second cycles were arbitrarily shifted for clarity. T_m [(a) 91.7°C, (b) 100.9°C, and (c) 126.2°C], T_{OOT} [(c) 190.5°C and 170.6°C], and T_g [(a) 84.0°C, (b) 80.0°C, and (c) 73.0°C] values are shown in red, gray, and blue, respectively.

In-situ SAXS experiments were performed to examine the morphology transitions of the PESxNa polymers with temperature. Figure 2 shows representative diffraction patterns at selected temperatures and more scattering data are provided in Figure S5. At 40 °C before heating, polymers show a diffraction peak at $q \sim 1.5$ Å⁻¹, corresponding to the [100] hexagonal lattice of crystalline polyethylene.³⁶ The areas of the crystalline peak and amorphous halo are integrated and indicate 33%, 42%, and 62% crystallinity for PES10Na, PES12Na, and PES18Na, respectively. At q < 0.7 Å⁻¹, the scattering peaks exhibit the ratio of 1:2 (q/q^*) indicating layered ionic aggregates, which are driven by the crystallization of the polyethylene blocks. Therefore, the higher crystallinity associated with longer polyethylene blocks gives rise to stronger higher-order peaks from the layered ionic aggregates. The d-spacing of these layers (d_L) increases with the length of polyethylene blocks as $d_L = 2\pi/q^* = 21.0$, 24.1, and 32.9 Å for PES10Na, PES12Na, and PES18Na, respectively. The difference of d_L for PES10Na and PES18Na (11.9 Å) is larger than the *all-trans* contour length difference of 10- and 18-carbons (10.0 Å), which corresponds to the lower crystallinity of the 10-carbon polyethylene blocks.

Upon heating above the melting temperature, both PES12Na and PES18Na transition to cubic gyroid ($Ia\bar{3}d$), whereas PES10Na transitions to hexagonal ionic aggregate morphologies. The melting of crystalline polyethylene blocks is indicated by the very broad peaks centered at $q \sim 1.5 \text{ Å}^{-1}$. It is notable that PES10Na and PES12Na, which differ by two methylene groups, have different phase transitions, indicating the sensitivity of nanoscale aggregate morphology on polymer composition. Further increases of temperature give rise to a gyroid to hexagonal transition in PES12Na and PES18Na, while the hexagonal morphology persists in PES10Na. The second order scattering peaks remain present in these hexagonal morphologies up to the maximum temperature studied (Figure S5). Selected ionic aggregate morphologies and lattice parameters of

PES10Na, PES12Na, and PES18Na are provided in Table 2. Upon cooling, the slow crystallization kinetics observed in DSC is also evident in the X-ray scattering. For example, within the timescale of the scattering experiment the amorphous HEX morphology of PES10Na persists to 40 °C and this polymer fails to transition into a crystalline layered morphology during *in-situ* cooling. For PES12Na and PES18Na, the HEX to GYR transitions is observed upon cooling, while the amorphous GYR morphologies persist below the melting temperatures. These polymers recrystallize at room temperature after longer times as previously reported for PES23Na¹⁷ and PES48Na¹⁸, and further evidenced by *ex-situ* X-ray scattering of PES12Na (Figure S6).

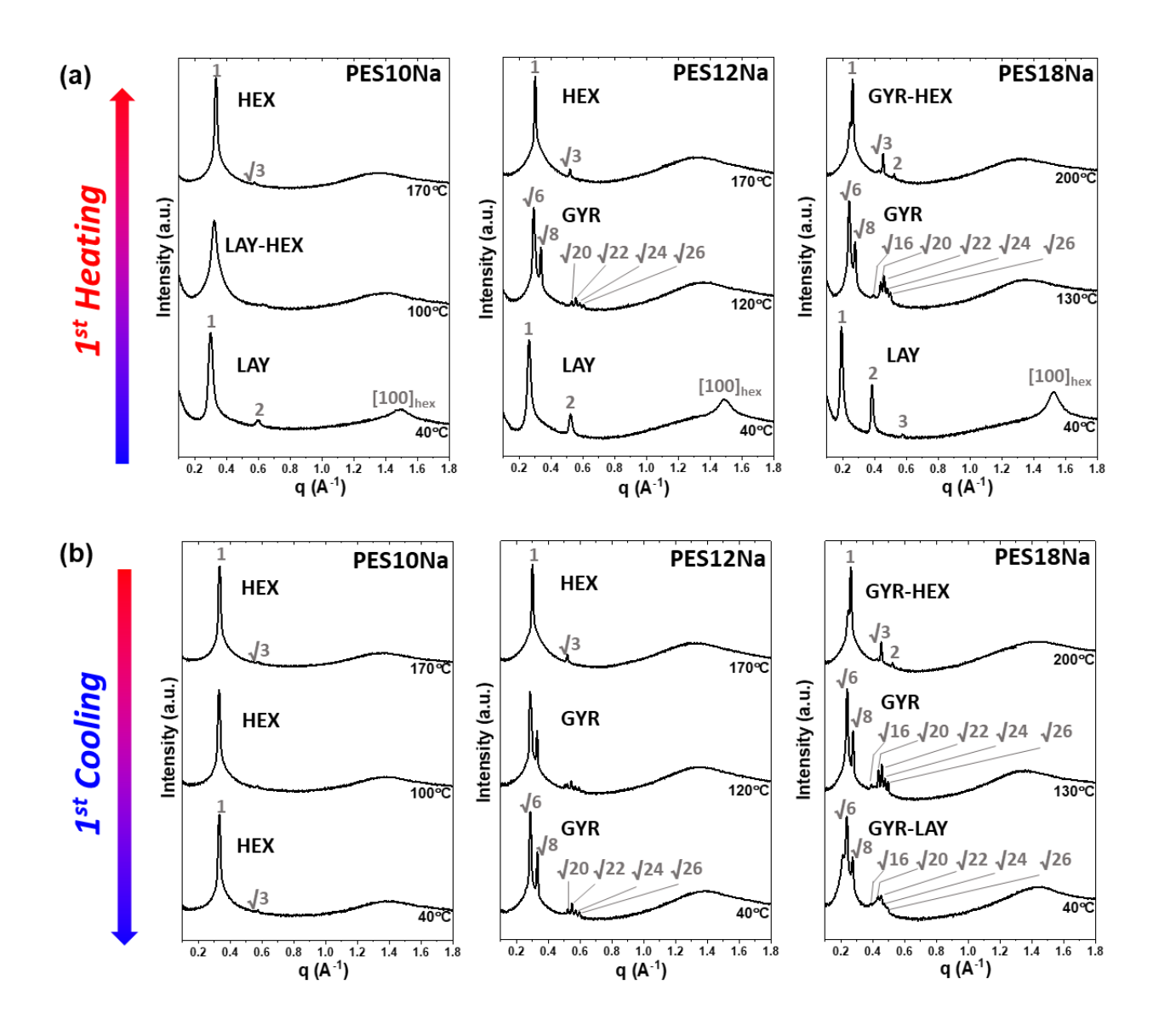


Figure 2. Representative *in-situ* SAXS patterns of PES10Na, PES12Na, and PES18Na measured at every 10°C while (a) heating and (b) cooling. The full scattering data are available in Figure S5. LAY, GYR, and HEX indicate layered, gyroid, and hexagonal ionic aggregate morphologies, respectively. The lattice parameters at selected temperatures are provided in Table 2.

Table 2. Ionic aggregate morphologies and lattice parameters of PES10Na, PES12Na, and PES18Na at selected temperatures as determined by *in-situ* SAXS data while heating.

Polymer	Temperature (°C)	Morphology	Lattice parameters (Å)
PES10Na	40	Layered	21.0
	170	Hexagonal	21.7
PES12Na	40	Layered	24.1

	120	Gyroid	53.1
	170	Hexagonal	24.2
PES18Na	40	Layered	32.9
	130	Gyroid	64.2
	200	Gyroid + Hexagonal	62.8 (GYR), 27.7 (HEX)

Table 3 summarizes thermal and morphological transitions of PES10Na, PES12Na, and PES18Na as determined by DSC and X-ray scattering. Given the inherent difference in their heating and cooling rates, there is excellent agreement between these two experimental methods with respect to the melting and order-order transition temperatures. For example, PES18Na exhibits an endothermic transition at 126.2°C that corresponds to the LAY to GYR morphology transition. Similarly, PES18Na exhibits GYR – HEX transitions upon heating and cooling in both DSC and X-ray scattering. Note that for PES12Na, X-ray scattering shows GYR – HEX transitions, which are not observed by DSC trace. This is attributed to the small enthalpic changes during the GYR – HEX transitions of PES12Na and will be discussed more below.³⁷

Table 3. Summary of thermal and morphological transitions of PES10Na, PES12Na, and PES18Na

Polymer		Heating		Cooling	
	$T_{\text{endo}} (^{\circ}C)^a$	T_{OOT} (°C) ^b	$T_{\text{exo}} (^{\circ}C)^a$	T_{OOT} (°C) ^b	
PES10Na	91.7	\sim 100; LAY \rightarrow HEX	-	-	
PES12Na	100.9	\sim 100; LAY \rightarrow GYR	-	-	

-	\sim 140; GYR \rightarrow HEX	-	\sim 130; HEX \rightarrow GYR
126.2	\sim 110 – 120; LAY \rightarrow GYR	-	-
190.5	\sim 180 – 190; GYR \rightarrow HEX	170.6	\sim 170 – 160; HEX \rightarrow GYR
	126.2	126.2 \sim 110 – 120; LAY \rightarrow GYR	10(0 110 100 1 111 0 111

^aThermal transition temperatures are from DSC trace (Figure 1). ^bThe morphology of ionic aggregates. Transition temperatures are estimated from *in-situ* SAXS measurements (Figure S5).

Morphology Maps and Phase Diagram

Morphology maps were constructed from *in-situ* X-ray scattering results using 1/T versus $f_{\rm polar}$. The data at $f_{\rm polar} \sim 0.16$ and 0.27 correspond to PES48Na and PES23Na, respectively, as previously reported. ^{17,18} In the morphology map constructed from the heating data (Figure 3a), layered ionic aggregates exhibit transitions at the melting temperatures to either hexagonal ($f_{
m polar}$ \sim 0.16 and 0.45) or gyroid ($f_{polar} \sim 0.27, 0.32$, and 0.41) morphologies. Since layered ionic aggregates are indicative of semicrystalline polyethylene, the first OOTs correspond to the melting of polymer backbones and are consistent with the melting transitions in the first-heating DSC data (Figure 1 and Table 3). Note that these melting transition temperatures decrease (1/T increase) with increasing f_{polar} , as consistent with less crystallinity due to shorter polyethylene blocks. As I/Tdecreases further, polymers with f_{polar} of 0.27, 0.32, and 0.41 form gyroid and further transition into hexagonal morphologies, while polymers with f_{polar} of 0.16 and 0.45 exhibit LAY – HEX transitions without the intermediate gyroid morphologies. This morphology map shows that the nanoscale ionic aggregates in PESxNa polymers vary with f_{polar} and temperature, demonstrating the presence of gyroid morphologies at intermediate temperatures and $0.27 \le f_{\text{polar}} \le 0.41$. When diblock copolymers exhibit the gyroid structure, the experimental composition window is typically narrower, ~ 4 vol%. 32 More research is needed to establish if the wider composition window for

the gyroid structure in PESxNa is the result of the multiblock architecture or a large χ_{eff} .

Figure 3b is the cooling morphology map of PESxNa and displays an expanded temperature range of gyroid morphologies due to slow crystallization kinetics. In our previous report, PES48Na ($f_{\text{polar}} \sim 0.16$) showed HEX to LAY transitions upon cooling in X-ray scattering, due to the strong crystallization driving forces associated with the long polyethylene blocks. In contrast, the gyroid morphology in PES23Na persisted for 3 days after cooling to room temperature, which is attributed to the slower crystallization kinetics of the shorter polyethylene blocks. In this study, we report that the new PESxNa polymers maintain their melt-state morphologies upon cooling, similar to PES23Na. Specifically, PES10Na maintains the hexagonal morphology, and PES12Na and PES18Na maintain their gyroid morphologies below the melting temperatures. In summary, upon cooling the melt morphologies of the PESxNa polymers with $f_{\text{polar}} > 0.27$ persist below T_{m} due to their slow crystallization behaviors.

A wide range of GYR-HEX coexistence for PES18Na is attributed to the strong polar interactions that slow OOT kinetics. In Figure S7, an isothermal X-ray scattering experiment for PES18Na shows the gradual transition from GYR and HEX to only HEX morphology after 9 hours at 200°C. The in-situ X-ray scattering experiments (Figure 2) held temperature for only 15 minutes before a 10-minute exposure. Thus, we conclude that the regions of GYR-HEX coexistence in Figure 3 result from the slow OOT kinetics of these polymers.

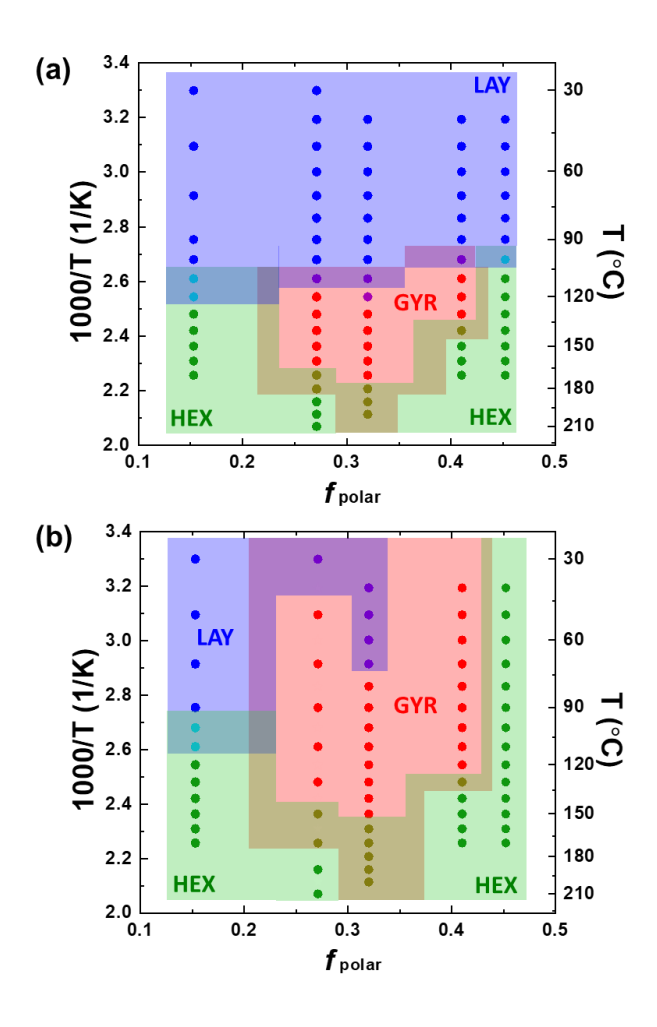


Figure 3. Morphology maps of PESxNa while (a) heating and (b) cooling plotted as I/T versus f_{polar} . LAY (blue), GYR (red), and HEX (green) indicate layered, gyroid, and hexagonal ionic aggregate morphologies. There are mixed phases near the transitions temperatures as indicated by light blue (LAY + HEX), purple (LAY + GYR), and olive (GYR + HEX) colors. Morphologies at $f_{\text{polar}} \sim 0.16$ and 0.27 are previously reported elsewhere. 17,18

The morphology maps clearly illustrate various OOTs and a broad gyroid region. Surprisingly, there are hexagonal - gyroid - hexagonal transitions with increasing f_{polar} at 130 °C < T < 180 °C, Figure 3a. This might suggest the appearance of an inverse hexagonal symmetry with increasing f_{polar} , although this is inconsistent with the f_{polar} < 0.5 in these multiblock copolymer electrolytes. Recall that phase diagrams of diblock copolymers use the product of χ (~I/T) and the total degree of polymerization on the y-axis, rather than just I/T as in Figure 3. For the multiblock

copolymers studied here, we employ the number of backbone atoms in a monomeric unit (N_m) , defined as $N_m = x + 6$. For PESxNa polymers, x and x are the number of backbone atoms of non-polar and polar groups, respectively (Scheme 1).

Figure 4 illustrates the phase diagram upon heating of PESxNa using N_m/T on the y-axis. This N_m/T versus f_{Polar} representation enables comparison with conventional diblock copolymers. Interestingly, the OOTs in PESxNa phase diagram exhibits a gyroid phase bounded by the hexagonal phases at lower N_m/T and bounded by the layered phase at higher N_m/T . While the layered morphology of conventional diblock copolymers is observed near the symmetric compositions, the layered ionic aggregate morphologies of PESxNa persist at $f_{\text{Polar}} \sim 0.16$ due to crystallization of the PESxNa polymers below the T_m . Note that order-to-disorder transitions (ODTs) were inaccessible in these PESxNa polymers due to polymer degradation, and are expected at a higher temperature (shown by the dashed line). This phase diagram clearly captures the OOTs of ordered ionic aggregate morphologies as a function of N_m/T and f_{Polar} , where N_m is defined by the monomeric repeat unit rather than the total degree of polymerization of these multiblock copolymers.

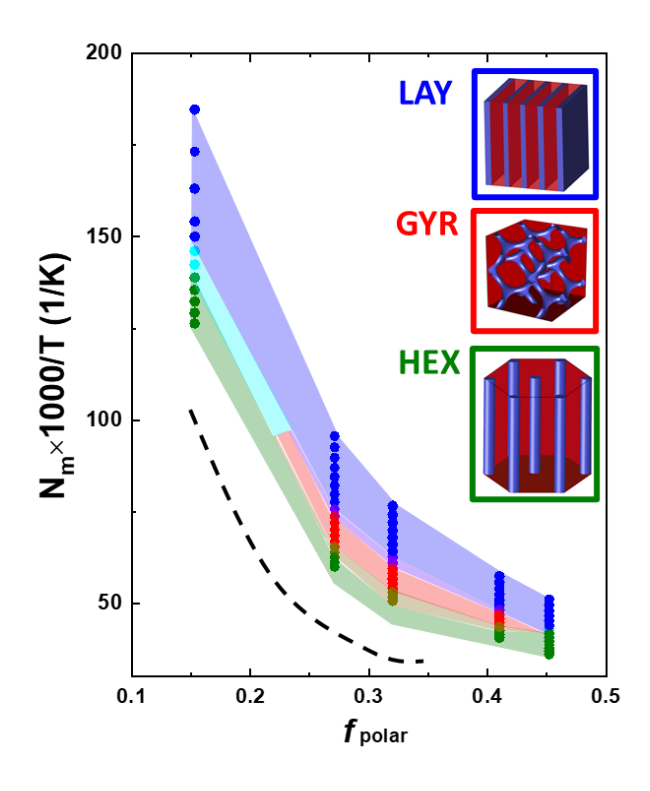


Figure 4. The N_m/T versus f_{polar} phase diagram for PESxNa polymers based on heating *in-situ* X-ray scattering data. The colored regions indicate the ionic aggregate morphologies as described in the Figure 3 caption. The dashed line represents an experimentally inaccessible order-to-disorder transition at higher temperatures.

To further justify the use of N_m in the phase diagram, we investigated the scaling between N_m and domain spacing of hexagonal ionic aggregate morphologies d_{HEX} . Figure 5 shows $d_{HEX} \sim N_m^{0.52}$ scaling for PESxNa polymers, indicating the domain spacings (20 - 50 Å) of nanoscale ionic aggregates is controlled by N_m . This matches the Gaussian chain model prediction of $d \sim N_m^{0.5}$ for weakly segregated and disordered systems of symmetric diblock copolymer melts; typically this scaling is experimentally inaccessible in weakly segregated systems due to fluctuation effects.^{38–40} Importantly, we note that the very short chains of the polar blocks in the PESxNa polymers is

incompatible with models assuming Gaussian chains. Nonetheless, this $d_{HEX} \sim N_m^{0.52}$ scaling indicates controllable interaggregate domain spacings at a sub-50 Å length scale and further supports the use of N_m for the phase diagram of PESxNa polymers.

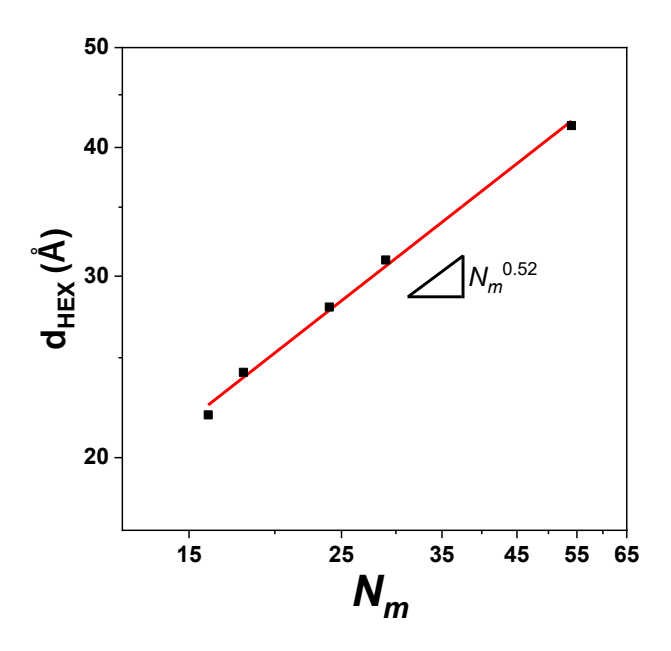


Figure 5. Domain spacings of hexagonal morphologies and its $N_m^{0.52}$ scaling. N_m is defined as x + 6 for PESxNa polymers. Domain spacings of all polymers are obtained from the q^* at 170 °C while cooling.

Block copolymer phase diagrams connect the microphase separated morphologies to the interactions between the blocks and the composition, and are valuable tools for designing block copolymers with specific self-assembled morphologies.³² To our knowledge, Figure 4 is the first experimental phase diagram of a multiblock copolymer electrolyte. Though there are a few theoretical,⁴¹ experimental,^{42–44} and simulation⁴⁵ studies that identify the ordered morphologies with neutral multiblock copolymers, our results are unique as we broadly map out various OOTs, including gyroid morphologies, with charge-containing multiblock copolymer electrolytes. Along

with the phase diagram and N_m -dependence of d_{HEX} , we have demonstrated that both the morphologies of ionic aggregates and the domain spacings can be fine-tuned by polymer design.

Morphology – Conductivity Relationships

Figure 6a presents the temperature- and morphology-dependent ionic conductivities of PES10Na, PES12Na, and PES18Na measured upon cooling. The ionic conductivity of PES23Na is included for comparison. ¹⁷ The conductivity profiles of all PESxNa polymers are well-described with Vogel-Fulcher-Tammann (VFT) relationship, suggesting the ion transport in PESxNa polymer melts is coupled to the polymer segmental relaxation. When the ion transport is decoupled from the polymer chain dynamics, as in a glassy or crystalline polymer matrix, the ionic conductivity shows Arrhenius-like temperature dependence.^{3,46} The VFT-fitting curves and parameters are provided in Figure S7 and Table S1, respectively. The fitting of PES18Na is performed below 130°C because the HEX − GYR transition leads to the conductivity plateau at ~140 - 160°C. In addition, the ionic conductivities of the PESxNa polymers decrease with shorter polyethylene segments (x) consistent with the increasing glass transition temperatures (T_g) , even though smaller x increases the ionic concentration. At 110°C, the ionic conductivity in the gyroid morphology of PES12Na is lower by an order of magnitude than that of PES23Na due to the higher T_g of PES12Na (~80°C) than PES23Na (~65°C). These VFT relationships and $T_g\mbox{-dependence}$ of ionic conductivities indicate that the ion transport behaviors are coupled to the polymer chain dynamics.

Ionic conductivities of PESxNa also depend on the ionic aggregate morphologies. For PES10Na and PES23Na, ionic conductivities decrease upon cooling and uniformly follow VFT relationships, because there are no morphological transitions during the measurements. In contrast,

the conductivity profile of PES18Na exhibits a plateau at the HEX – GYR transition (\sim 140 - 160 °C) upon cooling, and then exhibits a VFT relationship while in the gyroid morphology. This indicates higher ionic conductivities in gyroid morphologies than hexagonal morphologies, which is attributed to faster ion transport in the interconnected ionic aggregate channels of gyroid morphologies. For PES12Na, the ionic conductivities are described with a VFT relationship across the measured temperature range (Figure S8), although the ionic aggregate morphologies undergo a HEX – GYR transition upon cooling (Figure 2b and 3b). Recall that DSC failed to detect a thermal transition between the gyroid and hexagonal morphologies in PES12Na (Figure 1). Since the HEX - GYR transition in PES12Na involves a weaker enthalpic change, the ionic conductivity curve follows VFT behavior with comparable fragility strength coefficients for these two morphologies, $D_{\rm G} \approx D_{\rm H}$. Thus, these ionic conductivities of PESxNa demonstrate that ion transport is closely related to the ionic aggregate morphologies.

The T_g -normalized ionic conductivities of PESxNa highlight the morphological impact on ionic conductivities (Figure 6b). Notably, the ionic conductivities of PES12Na, PES18Na, and PES23Na overlap at $0.85 < T_g/T < 0.95$, which is the temperature range for the gyroid morphology. Also, PES10Na follows PES18Na at $T_g/T < 0.80$ corresponding to the hexagonal morphology. The collapse of T_g -normalized ionic conductivities further indicates the coupling of ion transport and polymer segmental relaxation, and thus VFT behavior. After accounting for segmental dynamics, higher ionic conductivities exist in the gyroid morphologies of PES12Na, PES18Na, and PES23Na rather than the hexagonal morphologies of PES10Na and PES18Na. At $T_g/T \sim 0.90$, ionic conductivities in gyroid morphologies of PES12Na, PES18Na, and PES23Na are higher than the ionic conductivity in hexagonal morphology of PES10Na by order of magnitude. These results demonstrate that the gyroid ionic aggregates are advantageous relative to hexagonal ionic

aggregates in these polymers.

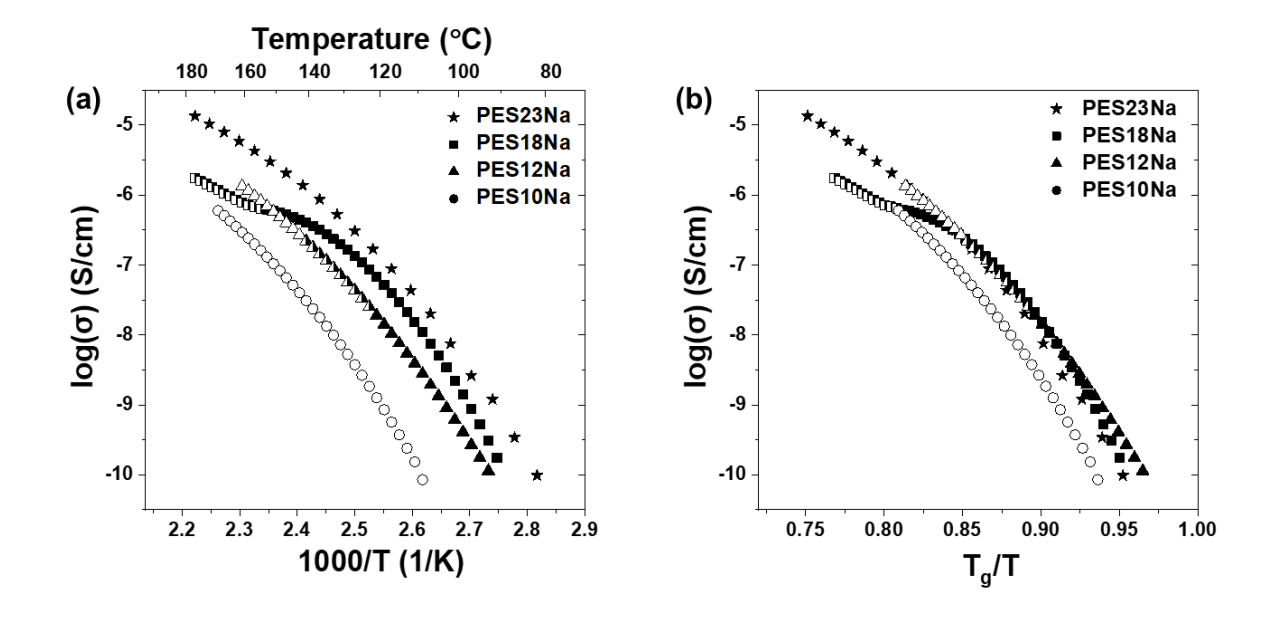


Figure 6. (a) Ionic conductivities and (b) T_g-normalized conductivities of PES10Na, PES12Na, and PES18Na measured upon cooling. The data for PES23Na are obtained from the reference. The filled and open symbols indicate the gyroid and hexagonal ionic aggregate morphologies, respectively, and half-filled symbols are mixed gyroid and hexagonal phases.

The ordered ionic aggregate morphologies have characteristic lengths (l) that provide further insights into the morphology-conductivity relationships. We define the characteristic lengths of the hexagonal, gyroid, and layered morphologies as $l_{\rm H} = \frac{2}{\sqrt{3}} d_{HEX(100)}$, $l_{\rm G} = \frac{2}{\sqrt{3}} d_{GYR(211)}$, and $l_{\rm L} = d_{LAY(100)}$, respectively. These lengths are topologically related when morphologies undergo OOTs. ^{47–49} Along with the persisting hexagonal morphologies in PES10Na upon cooling, $l_{\rm H,10Na}$ is constant at ~22Å upon cooling, Figure 7. For PES12Na, the HEX – GYR transition exhibits epitaxial relationships with ($l_{\rm G} - l_{\rm H}$) ~ 0.7Å at 130°C upon cooling, which corresponds to a smooth decrease in ionic conductivities (Figure 6). The absence of thermal transitions (via DSC) between the hexagonal and gyroid morphologies in PES12Na is also consistent with the epitaxial relationship between the two morphologies and a single VFT relationship over the measured

temperature range. This transition from hexagonally packed ionic aggregates to interconnected gyroid channels requires minimal polymer chain rearrangement such that the ionic conductivities are insensitive to the OOT. The difference between l_G and l_H in PES18Na is significantly larger (~2Å) indicating that the HEX – GYR transition involves a larger extent of polymer chain rearrangement. The hexagonal morphologies of PES18Na exhibit measurably lower ionic conductivities than the gyroid morphologies, because at this OOT the morphological transition is significant. The OOT in PES18Na is also apparent in DSC, Figure 1c. Our previous report of PES23Li identified an even larger disparity in ionic conductivities between gyroid and hexagonal morphologies along with a larger ($l_G - l_H$) ~ 5Å at the OOT.¹⁷ Due to the temperature limit in the EIS measurements, ionic conductivity at the HEX – GYR transition could not be studied for PES23Na, although both DSC and X-ray scattering indicate an OOT and the $l_G - l_H$ ~ 3.5Å.

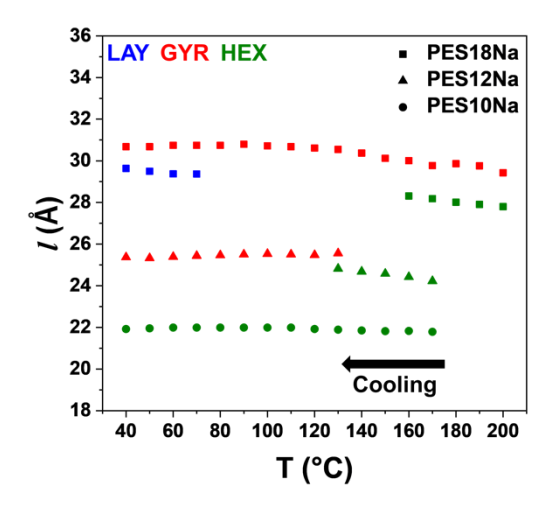


Figure 7. Characteristic lengths of ionic aggregate morphologies of PESxNa polymers upon cooling. The blue, red, and green colors indicate the layered, gyroid, and hexagonal morphologies, respectively. The characteristic lengths of morphologies are calculated from the primary X-ray scattering peak, q^* , and $d = 2\pi/q^*$; the equations for the characteristic lengths are given in the text.

Various self-assembled ion conductors have explored morphological effects on ionic conductivity, including layered, hexagonal, and gyroid morphologies.^{21,50–58} In polymerized ionic

liquids, grain boundaries significantly reduce the ionic conductivities in the mixed layered and hexagnoal morphologies.⁵⁰ In ionic liquid crystals^{51,52,58} and dendrites⁵³, the gyroid morphology exhibit a higher ionic conductivity than hexagonal morphology, and this is attributed to the bicontinous ion transport network of gyroid where the ions can migrate with a minimal impact of defects or grain boundaries. A PEO-based ternary blend with Li-salt shows a higher ionic conductivity through bicontinuous ion-conducting domains (C15 phase) than hexagonal domains.⁵⁴ For PESxNa, we observe more efficient ion transport through bicontinuous gyroid morphologies than hexagonal morphologies, and the conductivity differences are correlated to the characteristic lengths of the morphologies. Note that the grain size of the morphologies, as estimated from the peak width of X-ray scattering, is considerably larger (~10 to 38 times) than the microdomain structures (Table S2). Thus, we conclude that the conductivity differences in PESxNa mainly originate from the morphology types and characteristic lengths of ionic aggregates rather than the impact of grain boundaries.

These results demonstrate strong correlations between the phase behavior, nanoscale characteristic lengths of the ionic aggregates, and the ion transport properties for single-ion conducting multiblock copolymers. Also, we have established the boundaries of gyroid morphologies for PESxNa at a wide range of $0.27 < f_{polar} < 0.41$. Although the ionic conductivities of PESxNa are too low for practical applications, gyroidal ionic aggregate morphologies perform better than hexagonal morphologies in these multiblock copolymers, and further improvements are envisioned. For example, the sulfonate group can be replaced with a larger anionic group to increase cation dissociation and promote cation mobility. In addition, solvents, oligomers, or ionic liquids could be selectively infiltrated into the ionic aggregates (i.e. the polar microdomains) to improve cation dissociation and ionic conductivity.

CONCLUSION

Single-ion conducting polymer electrolytes (SIPEs) with ordered morphologies, including the bicontinuous gyroid, were investigated to build a fundamental understanding of design rules for efficient ion transport in multiblock copolymers. Using a set of five multiblock copolymer electrolytes with short polar blocks containing one SO₃-Na⁺ group and polyethylene blocks with precisely x carbons (PESxNa), we establish structure – property relationships. *In-situ* X-ray scattering experiments reveal order-to-order transitions (OOTs) in these polymers, and these OOTs are combined into a N_m/T vs f_{polar} phase diagram that successfully maps the phase transitions of PESxNa multiblock copolymers. This diagram, which is the first for a charged multiblock copolymer, highlights the ability to control the ionic aggregate morphologies using composition and T. The ordered morphologies of PESxNa reveal that the higher ionic conductivities in gyroid relative to hexagonal ionic aggregates are closely related to the characteristic lengths of these morphologies. Our results demonstrate faster ion transport through bicontinuous ionic aggregates than isotropic hexagonal morphologies in these multiblock copolymers, and provide future guidance for designing viable SIPEs with enhanced ionic conductivities. Next steps could include maintaining the gyroid morphologies at room temperature and increasing cation dissociation without perturbing the well-organized ionic aggregates. Moreover, these new insights about functional multiblock copolymers will encourage a broader investigation of step-growth polymerization to design self-assembled polymers for various potential applications.

AUTHOR INFORMATION

Corresponding Authors

*E-mail: stefan.mecking@uni.kn

*E-mail: winey@seas.upenn.edu

ORCID

Jinseok Park: 0000-0002-0389-9707

Anne Staiger: 0000-0002-6103-4402

Stefan Mecking: 0000-0002-6618-6659

Karen I. Winey: 0000-0001-5856-3410

Author Contributions

§J.P. and A.S. contributed equally to this work.

Notes

The authors declare no competing financial interest.

ACKNOWLEDGMENTS

J.P. and K.I.W. acknowledge funding by the National Science Foundation (DMR 1904767). J.P.

acknowledges a graduate student fellowship from the Vagelos Institute for Energy Science and

Technology at the University of Pennsylvania. J.P. and K.I.W. also acknowledge the use of the

Dual Source and Environmental X-ray Scattering facility operated by the Laboratory for Research

on the Structure of Matter at the University of Pennsylvania (NSF MRSEC 17-20530). The

equipment purchase was made possible by an NSF MRI grant (17-25969), an ARO DURIP grant

30

(W911NF-17-1-0282), and the University of Pennsylvania. A.S. and S.M. gratefully acknowledge funding by the Stiftung Baden-Württemberg (PRICON) and support by the DFG (SFB 1214, Particle analysis center and project A8).

ASSOCIATED CONTENT

Supporting Information Available: Calculation of DP_n from NMR spectra, full *in-situ* X-ray scattering data of PES10Na, PES12Na, and PES18Na. *Ex-situ* X-ray scattering data of PES12Na. Isothermal X-ray scattering experiments of PES18Na. VFT fitting and fitting parameters for ionic conductivity of PES10Na, PES12Na, and PES18Na. Correlation length and lattice parameter of PES10Na, PES12Na, and PES18Na. This material is available free of charge *via* the Internet at http://pubs.acs.org.

REFERENCES

- (1) Manthiram, A.; Yu, X.; Wang, S. Lithium Battery Chemistries Enabled by Solid-State Electrolytes. *Nat. Rev. Mater.* **2017**, *2*, 1–16.
- (2) Mindemark, J.; Lacey, M. J.; Bowden, T.; Brandell, D. Beyond PEO—Alternative Host Materials for Li+-Conducting Solid Polymer Electrolytes. *Prog. Polym. Sci.* **2018**, *81*, 114–143.
- (3) Bocharova, V.; Sokolov, A. P. Perspectives for Polymer Electrolytes: A View from Fundamentals of Ionic Conductivity. *Macromolecules* **2020**, *53*, 4141–4157.
- (4) Wanakule, N. S.; Panday, A.; Mullin, S. A.; Gann, E.; Hexemer, A.; Balsara, N. P. Ionic Conductivity of Block Copolymer Electrolytes in the Vicinity of Order-Disorder and Order-Order Transitions. *Macromolecules* **2009**, *42*, 5642–5651.
- (5) Teran, A. A.; Mullin, S. A.; Hallinan, D. T.; Balsara, N. P. Discontinuous Changes in Ionic Conductivity of a Block Copolymer Electrolyte through an Order-Disorder Transition. *ACS Macro Lett.* **2012**, *1*, 305–309.
- (6) Lodge, T. P.; Xie, S.; Lindsay, A. P.; Bates, F. S. Formation of a C15 Laves Phase with a Giant Unit Cell in Salt-Doped A/B/Ab Ternary Polymer Blends. *ACS Nano* **2020**, *14*, 13754–13764.
- (7) Ma, Q.; Zhang, H.; Zhou, C.; Zheng, L.; Cheng, P.; Nie, J.; Feng, W.; Hu, Y.; Li, H.; Huang, X.; et al. Single Lithium-Ion Conducting Polymer Electrolytes Based on a Super-Delocalized Polyanion Angewandte. *Angew. Chemie Int. Ed.* **2016**, *53*, 2521–2525.
- (8) Zhang, H.; Li, C.; Piszcz, M.; Coya, E.; Rojo, T.; Rodriguez-Martinez, L. M.; Armand, M.; Zhou, Z. Single Lithium-Ion Conducting Solid Polymer Electrolytes: Advances and Perspectives. *Chem. Soc. Rev.* **2017**, *46*, 797–815.
- (9) Diederichsen, K. M.; McShane, E. J.; McCloskey, B. D. Promising Routes to a High Li+ Transference Number Electrolyte for Lithium Ion Batteries. *ACS Energy Lett.* **2017**, *2*, 2563–2575.
- (10) Schauser, N. S.; Grzetic, D. J.; Tabassum, T.; Kliegle, G. A.; Le, M. L.; Susca, E. M.; Antoine, S.; Keller, T. J.; Delaney, K. T.; Han, S.; et al. The Role of Backbone Polarity on Aggregation and Conduction of Ions in Polymer Electrolytes. *J. Am. Chem. Soc.* **2020**, *142*, 7055–7065.
- (11) Feng, S.; Shi, D.; Liu, F.; Zheng, L.; Nie, J.; Feng, W. Single Lithium-Ion Conducting Polymer Electrolytes Based on Poly[(4-Styrenesulfonyl)(Trifluoromethanesulfonyl)Imide] Anions. *Electrochim. Acta* **2013**, *93*, 254–263.
- (12) Diederichsen, K. M.; Buss, H. G.; McCloskey, B. D. The Compensation Effect in the Vogel-Tammann-Fulcher (VTF) Equation for Polymer-Based Electrolytes. *Macromolecules* **2017**, 50, 3831–3840.
- (13) Webb, M. A.; Jung, Y.; Pesko, D. M.; Savoie, B. M.; Yamamoto, U.; Coates, G. W.; Balsara,

- N. P.; Wang, Z. G.; Miller, T. F. Systematic Computational and Experimental Investigation of Lithium-Ion Transport Mechanisms in Polyester-Based Polymer Electrolytes. *ACS Cent. Sci.* **2015**, *1*, 198–205.
- (14) Ebadi, M.; Eriksson, T.; Mandal, P.; Costa, L. T.; Araujo, C. M.; Mindemark, J.; Brandell, D. Restricted Ion Transport by Plasticizing Side Chains in Polycarbonate-Based Solid Electrolytes. *Macromolecules* **2020**, *53*, 764–774.
- (15) Kang, S.; Park, M. J. 100th Anniversary of Macromolecular Science Viewpoint: Block Copolymers with Tethered Acid Groups: Challenges and Opportunities. *ACS Macro Lett.* **2020**, 1527–1541.
- (16) Park, M. J. Confinement-Entitled Morphology and Ion Transport in Ion-Containing Polymers. *Mol. Syst. Des. Eng.* **2019**, *4*, 239–251.
- (17) Yan, L.; Rank, C.; Mecking, S.; Winey, K. I. Gyroid and Other Ordered Morphologies in Single-Ion Conducting Polymers and Their Impact on Ion Conductivity. *J. Am. Chem. Soc.* **2020**, *142*, 857–866.
- (18) Rank, C.; Yan, L.; Mecking, S.; Winey, K. I. Periodic Polyethylene Sulfonates from Polyesterification: Bulk and Nanoparticle Morphologies and Ionic Conductivities. *Macromolecules* **2019**, *52*, 8466–8475.
- (19) Yan, L.; Hauler, M.; Bauer, J.; Mecking, S.; Winey, K. I. Monodisperse and Telechelic Polyethylenes Form Extended Chain Crystals with Ionic Layers. *Macromolecules* **2019**, *52*, 4949–4956.
- (20) Zhai, C.; Zhou, H.; Gao, T.; Zhao, L.; Lin, S. Electrostatically Tuned Microdomain Morphology and Phase-Dependent Ion Transport Anisotropy in Single-Ion Conducting Block Copolyelectrolytes. *Macromolecules* **2018**, *51*, 4471–4483.
- (21) Shen, K. H.; Brown, J. R.; Hall, L. M. Diffusion in Lamellae, Cylinders, and Double Gyroid Block Copolymer Nanostructures. *ACS Macro Lett.* **2018**, *7*, 1092–1098.
- (22) Evans, C. M.; Bridges, C. R.; Sanoja, G. E.; Bartels, J.; Segalman, R. A. Role of Tethered Ion Placement on Polymerized Ionic Liquid Structure and Conductivity: Pendant versus Backbone Charge Placement. *ACS Macro Lett.* **2016**, *5*, 925–930.
- (23) Kim, O.; Kim, K.; Choi, U. H.; Park, M. J. Tuning Anhydrous Proton Conduction in Single-Ion Polymers by Crystalline Ion Channels. *Nat. Commun.* **2018**, *9*, 1–8.
- (24) Park, M. J.; Balsara, N. P. Phase Behavior of Symmetric Sulfonated Block Copolymers. *Macromolecules* **2008**, *41*, 3678–3687.
- (25) Trigg, E. B.; Gaines, T. W.; Maréchal, M.; Moed, D. E.; Rannou, P.; Wagener, K. B.; Stevens, M. J.; Winey, K. I. Self-Assembled Highly Ordered Acid Layers in Precisely Sulfonated Polyethylene Produce Efficient Proton Transport. *Nat. Mater.* 2018, 17, 725–731.
- (26) Yoshida-hirahara, M.; Takahashi, S.; Yoshizawa-fujita, M.; Takeoka, Y.; Rikukawa, M. Synthesis and Investigation of Sulfonated Poly(p-Phenylene)-Based Ionomers with Precisely Controlled Ion Exchange Capacity for Use as Polymer Electrolyte Membranes. *RSC Adv.* **2020**, *10*, 12810–12822.

- (27) Kreuer, K. D. On the Development of Proton Conducting Polymer Membranes for Hydrogen and Methanol Fuel Cells. *J. Memb. Sci.* **2001**, *185*, 29–39.
- (28) Blachot, J.-F.; Diat, O.; Putaux, J.; Rollet, A.; Rubatat, L.; Vallois, C.; Müller, M.; Gebel, G. Anisotropy of Structure and Transport Properties in Sulfonated Polyimide Membranes. *J. Memb. Sci.* **2003**, *214*, 31–42.
- (29) Essafi, W.; Gebel, G.; Mercier, R. Sulfonated Polyimide Ionomers: A Structural Study. *Macromolecules* **2004**, *37*, 1431–1440.
- (30) Sing, C. E.; Zwanikken, J. W.; Olvera De La Cruz, M. Electrostatic Control of Block Copolymer Morphology. *Nat. Mater.* **2014**, *13*, 694–698.
- (31) Shim, J.; Bates, F. S.; Lodge, T. P. Superlattice by Charged Block Copolymer Self-Assembly. *Nat. Commun.* **2019**, *10*, 1–7.
- (32) Bates, F. S.; Fredrickson, G. H. Block Copolymers-Designer Soft Materials. *Phys. Today* **1999**, *52*, 32–38.
- (33) Trigg, E. B.; Tiegs, B. J.; Coates, G. W.; Winey, K. I. High Morphological Order in a Nearly Precise Acid-Containing Polymer and Ionomer. *ACS Macro Lett.* **2017**, *6*, 947–951.
- (34) Seitz, M. E.; Chan, C. D.; Opper, K. L.; Baughman, T. W.; Wagener, K. B.; Winey, K. I. Nanoscale Morphology in Precisely Sequenced Poly(Ethylene- Co -Acrylic Acid) Zinc Ionomers. *J. Am. Chem. Soc.* **2010**, *132*, 8165–8174.
- (35) Ortmann, P.; Heckler, I.; Mecking, S. Physical Properties and Hydrolytic Degradability of Polyethylene-like Polyacetals and Polycarbonates. *Green Chem.* **2014**, *16*, 1816–1827.
- (36) Tsubakihara, S.; Nakamura, A.; Yasuniwa, M. Hexagonal Phase of Polyethylene Fibers under High Pressure. *Polym. J.* **1991**, *23*, 1317–1324.
- (37) Floudas, G.; Ulrich, R.; Wiesner, U.; Chu, B. Nucleation and Growth in Order-to-Order Transitions of a Block Copolymer. *Europhys. Lett.* **2000**, *50*, 182–188.
- (38) Matsen, M. W.; Bates, F. S. Unifying Weak- and Strong-Segregation Block Copolymer Theories. *Macromolecules* **1996**, *29*, 1091–1098.
- (39) Barrat, J.; Fredrickson, G. H. Collective and Single-Chain Correlations near the Block Copolymer Order Disorder Transition. *J. Chem. Phys.* **1999**, *95*, 1281.
- (40) Mayes, A. M.; Cruz, M. O. De. Concentration Fluctuation Effects on Disorder Order Transitions in Block Copolymer Melts. *J. Chem. Phys.* **1999**, *95*, 4670.
- (41) Matsen, M. W. Effect of Architecture on the Phase Behavior of AB-Type Block Copolymer Melts. *Macromolecules* **2012**, *45*, 2161–2165.
- (42) Zeng, D.; Gupta, R.; Coughlin, E. B.; Hayward, R. C. Assembly of Disordered Cocontinuous Morphologies by Multiblock Copolymers with Random Block Sequence and Length Dispersity. *ACS Appl. Polym. Mater.* **2020**, *2*, 3282–3290.
- (43) Lee, I.; Panthani, T. R.; Bates, F. S. Sustainable Poly(Lactide-b-Butadiene) Multiblock Copolymers with Enhanced Mechanical Properties. *Macromolecules* **2013**, *46*, 7387–7398.

- (44) Panthani, T. R.; Bates, F. S. Crystallization and Mechanical Properties of Poly(1-Lactide)-Based Rubbery/Semicrystalline Multiblock Copolymers. *Macromolecules* **2015**, *48*, 4529–4540.
- (45) Li, S.; Xu, Q.; Li, K.; Yu, C.; Zhou, Y. High-χ Alternating Copolymers for Accessing Sub-5 Nm Domains via Simulations. *Phys. Chem. Chem. Phys.* **2020**, *22*, 5577–5583.
- (46) Paren, B. A.; Thurston, B. A.; Neary, W. J.; Kendrick, A.; Kennemur, J. G.; Stevens, M. J.; Frischknecht, A. L.; Winey, K. I. Percolated Ionic Aggregate Morphologies and Decoupled Ion Transport in Precise Sulfonated Polymers Synthesized by Ring-Opening Metathesis Polymerization. *Macromolecules* **2020**, *53*, 8960–8973.
- (47) Faunce, C. A.; Paradies, H. H. Two New Colloidal Crystal Phases of Lipid A-Monophosphate: Order-to-Order Transition in Colloidal Crystals. *J. Chem. Phys.* **2009**, *131*, 244708.
- (48) Llandro, J.; Love, D. M.; Kovács, A.; Caron, J.; Vyas, K. N.; Kákay, A.; Salikhov, R.; Lenz, K.; Fassbender, J.; Scherer, M. R. J.; et al. Visualizing Magnetic Structure in 3d Nanoscale Ni-Fe Gyroid Networks. *Nano Lett.* **2020**, *20*, 3642–3650.
- (49) Schulz, M. F.; Bates, F. S. Epitaxial Relationship for Hexagonal-to-Cubic Phase Transition in a Block Copolymer Mixture. *Phys. Rev. Lett.* **1994**, *73*, 86–89.
- (50) Weber, R. L.; Ye, Y.; Schmitt, A. L.; Banik, S. M.; Elabd, Y. A.; Mahanthappa, M. K. Effect of Nanoscale Morphology on the Conductivity of Polymerized Ionic Liquid Block Copolymers. *Macromolecules* **2011**, *44*, 5727–5735.
- (51) Ichikawa, T.; Yoshio, M.; Hamasaki, A.; Mukai, T.; Ohno, H.; Kato, T. Self-Organization of Room-Temperature Ionic Liquids Exhibiting Liquid-Crystalline Bicontinuous Cubic Phases: Formation of Nano-Ion Channel Networks. *J. Am. Chem. Soc.* **2007**, *129*, 10662–10663.
- (52) Ichikawa, T.; Yoshio, M.; Hamasaki, A.; Taguchi, S.; Liu, F.; Zeng, X. B.; Ungar, G.; Ohno, H.; Kato, T. Induction of Thermotropic Bicontinuous Cubic Phases in Liquid-Crystalline Ammonium and Phosphonium Salts. *J. Am. Chem. Soc.* **2012**, *134*, 2634–2643.
- (53) Cho, B. K.; Jain, A.; Gruner, S. M.; Wiesner, U. Mesophase Structure-Mechanical and Ionic Transport Correlations in Extended Amphiphilic Dendrons. *Science* (80-.). **2004**, 305, 1598–1601.
- (54) Xie, S.; Lindsay, A. P.; Bates, F. S.; Lodge, T. P. Formation of a C15 Laves Phase with a Giant Unit Cell in Salt-Doped A/B/AB Ternary Polymer Blends. *ACS Nano* **2020**.
- (55) Jo, G.; Ahn, H.; Park, M. J. Simple Route for Tuning the Morphology and Conductivity of Polymer Electrolytes: One End Functional Group Is Enough. *ACS Macro Lett.* **2013**, *2*, 990–995.
- (56) Kim, O.; Kim, S. Y.; Ahn, H.; Kim, C. W.; Rhee, Y. M.; Park, M. J. Phase Behavior and Conductivity of Sulfonated Block Copolymers Containing Heterocyclic Diazole-Based Ionic Liquids. *Macromolecules* **2012**, *45*, 8702–8713.
- (57) Kerr, R. L.; Miller, S. A.; Shoemaker, R. K.; Elliott, B. J.; Gin, D. L. New Type of Li Ion Conductor with 3D Interconnected Nanopores via Polymerization of a Liquid Organic

- Electrolyte-Filled Lyotropic Liquid-Crystal Assembly. J. Am. Chem. Soc. 2009, 131, 15972–15973.
- (58) Ichikawa, T.; Yoshio, M.; Hamasaki, A.; Kagimoto, J.; Ohno, H.; Kato, T. 3D Interconnected Ionic Nano-Channels Formed in Polymer Films: Self-Organization and Polymerization of Thermotropic Bicontinuous Cubic Liquid Crystals. *J. Am. Chem. Soc.* **2011**, *133*, 2163–2169.